Use of a Three-Dimensional Detailed Modeling Approach for Predicting Root Water Uptake

Mathieu Javaux,* Tom Schröder, Jan Vanderborght, and Harry Vereecken

We studied water uptake variability at the plant scale using a three-dimensional detailed model. Specifically, we investigated the sensitivity of the R-SWMS model under different plant collar conditions by comparing computed water fluxes, flow variability, and soil water distributions for different case scenarios and different parameterizations. The relative radial root conductivity and soil hydraulic conductivity were shown to control the plant water extraction distribution. Highly conductive soils promote water uptake but at the same time decrease the variability of the soil water content. A large radial root conductivity increases the amount of water extracted by the root and generates very heterogeneous water extraction profiles. Increasing the xylem conductivity has less impact because the xylem is generally the most conductive part of the system. It was also determined that, due to the different magnitudes of soil and root conductivities, similar one-dimensional sink-term profiles can result in very different water content and flux distributions at the plant scale. Furthermore, an analysis based on soil texture showed that the ability of a soil to sustain high plant transpiration demand cannot be predicted a priori from the soil hydraulic properties only, as it depends on the evaporative demand and on the three-dimensional distributions of the soil/root conductivity ratio and soil capacity, which continuously evolve with time. Combining soil and root hydraulic properties led to very complex one-dimensional sink functions that are quite different from the simple reduction functions usually found in the literature. The R-SWMS model could be used to develop more realistic one-dimensional reduction functions.

ABBREVIATIONS: CBC, collar boundary condition; RLD, root length density.

R OOT WATER UPTAKE is an important mechanism that dramatically affects the spatiotemporal water content distribution in the upper layers of vegetated soils; however, root water uptake processes and their interactions with soil are still poorly understood. One reason for this lack of understanding is the intrinsic difficulty of observing belowground processes and assessing soil and root properties. Another reason is the knowledge gap in understanding biological processes governing water extraction by roots. New advances in plant biology and the extended use of noninvasive techniques have opened new avenues for investigating more deeply root water uptake in relation to three-dimensional root architecture and soil variability.

M. Javaux, J. Vanderborght, and H. Vereecken, Institute for Chemistry and Dynamics of the Geosphere, Agrosphere Institute, ICG-IV, Forschungszentrum Juelich GmbH, D-52425 Juelich, Germany; and T. Schröder, Julich Supercomputing Center, Forschungszentrum Juelich GmbH, D-52425 Juelich, Germany. M. Javaux also Dep. of Environmental Sciences and Land Use Planning, Université Catholique de Louvain, Croix du Sud, 2, bte 2, B-1348 Louvain-la-Neuve, Belgium. Received 16 June 2007. *Corresponding author (mathieu.javaux@uclouvain.be).

Lynch (1995) pointed out that root architecture is a primary aspect of plant productivity, particularly in environments where water and nutrients are scarce. The actual root architecture of one plant is the result of a tradeoff between maximizing the soil explored for water and nutrients and minimizing the cost of energy and C transport (Fitter, 1987). On the other hand, root architecture also influences soil moisture and nutrient distributions at the plant scale. Although the impact of one-dimensional root distributions on soil water content depletion profiles has been shown in numerous studies, the complete root architecture and the root hydraulic properties are also of importance for assessing the three-dimensional variability of water distribution (Garrigues et al., 2006).

The need for more detailed models is also driven by practical purposes. Green et al. (2006) stressed that spatially variable models are needed as we become more precise in our application of water, fertilizers, and pesticides to the soil. They suggested that current methods to save water, "such as deficit irrigation and partial root zone drying […] will require that root models incorporate local variations in water content" (Green et al., 2006, p. 172).

Early modeling efforts focused on one-dimensional effective root water uptake models (Cowan, 1965; Gardner, 1960), whereas more recently modelers have considered two-dimensional (de Jong van Lier et al., 2006; Bruckler et al., 2004) and three-dimensional modeling approaches (Clausnitzer and Hopmans, 1994; Vrugt et al., 2001) that involve a higher level of complexity in the description of root structure and related soil and plant processes. Doussan et al. (2006) coupled water flow in the soil and within the root xylem by solving both domains iteratively.

Recently, we developed R-SWMS, a three-dimensional coupled water flow model for soil and roots with an uptake stress function, which couples the model of Somma et al. (1998) with the model of Doussan et al. (1998). Because water uptake and flow in soil and roots are driven by potential gradients, these models implicitly assume that soil water is preferably taken up at spatial locations where the energy to bring water to the root collar is minimized. These types of models are therefore great tools for checking hypotheses regarding root permeability and plant architectural adaptation to water availability, and for assessing the effect of plant genotype on uptake and solute transport (de Dorlodot et al., 2007).

One major drawback of three-dimensional models is the potentially large number of root and soil input parameters. On the other hand, compared with one-dimensional models, R-SWMS relies on more realistic assumptions for predicting root–soil interactions. First, the root architecture is explicitly taken into account, and root properties can differ for each root node. Plants have a variety of root types with different functions and hydraulic characteristics, which significantly affects the water uptake distribution. Recently, Pierret et al. (2007) emphasized the need for models that explicitly represent root architecture and discriminate between different root types. Second, horizontal variability is explicitly modeled. Even with uniform horizontal soil properties, horizontal water content variability may arise due to contrasting uptake by different root segments and redistribution processes. Third, water uptake is a passive process driven by the potential gradient between soil and root. The simulation of this process by R-SWMS, coupled with the ability to specify heterogeneous properties for both soil and root segments, allows the explicit modeling of the spatiotemporal variations of root water uptake.

Three-dimensional models permit the assessment of horizontal flow variability at the plant scale. It is therefore expected that these models can provide more realistic predictions of effective one-dimensional uptake time series, which could be used to develop new equations for effective one-dimensional sink terms and their time evolution. It is important, however, to first investigate how the three-dimensional model reacts to changes in root and soil parameters, especially plant hydraulic properties, and what data sets may be useful for investigating root water uptake processes.

In this study, we investigated the potential using a detailed model for studying water variability at the plant scale. This study investigated the sensitivity of the R-SWMS model under different plant collar conditions by comparing water fluxes, flow variability, and soil water distributions for different scenarios and parameterizations. We particularly considered the effect of the xylem conductivity, the root radial conductivity, and the soil hydraulic conductivity on the water uptake process. Effective one-dimensional sink terms were extracted from the three-dimensional simulations and the existence of effective plant behavior for specific hydraulic parameterizations was investigated.

Theory

Description of R-SWMS Model

The R-SWMS is a numerical model for predicting soil–root water fluxes based on the water potential gradient between soil and root nodes. Water flow is described by the Richards equation with a three-dimensional sink term:

$$\frac{\partial \theta}{\partial t} = \nabla \cdot \left[\mathbf{K} \nabla (h - z) \right] - S \qquad [1]$$

where θ is the volumetric water content [$L^3 L^{-3}$], t is time [T], $\mathbf{K}$ is the hydraulic conductivity tensor [LT^{-1}], h is the water potential on a weight basis [L], S is a sink term representing root water uptake [T^{-1}], and z is the vertical coordinate [L]. We used the method developed by Simunek et al. (1995) for solving the water potential in the soil.

Water flow within the root xylem and between the soil–root interface and root xylem is solved by discretizing the root system as a network of connected root nodes. One-dimensional radial (soil–root) flow, J_r, and axial (xylem) flow, J_x, are defined as

$$J_r = K_r^* s_r \left[h_s(z) - h_x(z) \right] \qquad [2a]$$

$$J_x = -K_x \left(\frac{\Delta h_x}{l} + \frac{\Delta z}{l} \right) \qquad [2b]$$

where h_s and h_x are the water potentials (on a weight basis) at the root surface and in the xylem [L], respectively, K_r^* is the intrinsic radial conductivity [T^{-1}], s_r is the outer surface of the root segment [L^2], l is the root segment length [L], and K_x is the xylem conductivity [$L^3 T^{-1}$]. Equations [2a] and [2b] are based on the assumption that the osmotic potential is negligible and that the root water capacity can be neglected. These assumptions are valid under normal conditions, i.e., no extreme water stress. The steady-state assumption is valid for small time steps. Equations [2a] and [2b] can be written for each of the root nodes, and the total system of equations can be solved in terms of water potential provided that the root boundary condition and the soil water potential around the root nodes are known.

Boundary conditions for roots are defined at the root collar and may be specified in terms of water potential or water flux. In the case of flux-type boundary conditions, stress may occur when the evaporative demand cannot be met by the soil. In such a case, a maximum allowable threshold value for absolute water potential h_{lim} is defined, beyond which the collar boundary condition (CBC) is automatically switched from a flux-type to a pressure-head-type condition with $|h| = |h_{lim}|$.

We adapted the model of Somma et al. (1998) to solve iteratively the soil (Eq. [1]) and root network flow equations for the water potential. These equations are linked by the soil–root radial fluxes (Eq. [2a]). Radial fluxes of root segments i located in a soil voxel j are summed to give the sink term S in Eq. [1]:

$$S_j = \frac{\sum_i^{n_i} J_{r,i}}{V_j} \qquad [3]$$

where V_j is the voxel volume and n_i is the number of root segments within voxel j.

The root model is first solved based on the initial soil water potential (h_s in Eq. [2a]) obtained from a distance-weighted average of calculated soil water potential at the corners of the soil voxels including root segments. A sink term is calculated for each soil node using Eq. [3] and inserted in Eq. [1] to solve soil water flow. Iterations are performed until soil water potential and moisture content converge below a threshold value.

Methodology

Scenario Descriptions

All of the simulations in this study feature a root structure located in the center of a cubic soil column measuring 10 by 10 by 40 cm, composed of 1-cm^3 voxels. The soil is initially in hydrostatic equilibrium with an aquifer located 300 cm below the surface. The boundary conditions for the soil are no rainfall or evaporation at the surface and no flux at the bottom of the soil column. The soil is homogeneous.

The root structure is defined with the model of Somma et al. (1998) as a root 500 h old, made of 9488 root segments, and grown in a homogeneous soil. Root hydraulic parameters for the reference scenario were taken from Doussan et al. (1998) and are typical for a maize (*Zea mays* L.) root: $K_x = 0.0432$ cm^3 d^{-1} and $K_r^* = 1.728 \times 10^{-4}$ d^{-1}. We considered these parameters uniform and constant throughout the root system. The limiting water potential was defined as $h_{lim} = -150$ m. No root growth was considered. These simplistic and artificial assumptions will help assess the behavior of the model as a first approximation.

Three principal boundary conditions at the root collar were used in this study: constant water potential (referred to as CBC 1), constant flux (CBC 2), and sinusoidal day–night fluxes (CBC 3). Table 1 summarizes the principal features of these reference CBCs.

Sensitivity Analysis of Conductivity Values with Collar Boundary Conditions 1 and 2

Water takes the least resistive pathway to reach the plant collar from the soil. Therefore, soil conductivity and root radial and axial conductivities are key parameters affecting model response. Consequently, our first analysis was of the model sensitivity to root and soil conductivities.

Table 2 gives the soil and root parameters used in this study. The reference soil for the sensitivity analysis is a loam with Mualem–van Genuchten parameters: residual and saturated volumetric water content $\theta_r = 0.078$ and $\theta_s = 0.43$, respectively; shape parameters $\alpha = 0.036$ cm^{-1} and $n = 1.56$; $m = 1 - 1/n$; soil saturated hydraulic conductivity, $K_{sat} = 24.96$ cm d^{-1}; and pore connectivity parameter $\lambda = 0.5$ (Carsel and Parrish, 1988). In the following, we refer to *reference scenarios* for simulations performed with the parameterization described in the first column of Table 2. Other cases use the same parameters except root parameters K_r^* or K_x, or soil K_{sat} are multiplied by 10 (second column of

TABLE 2. Model input reference and varied parameters.†

Substrate	Reference parameterization	Perturbed parameterization (multiplied by 10)
Loam soil	$\theta_r = 0.078$ $\theta_s = 0.43$ $\alpha = 0.036$ cm^{-1} $n = 1.56$ $\lambda = 0.5$ $K_{sat} = 24.96$ cm d^{-1}	$K_{sat} = 249.6$ cm d^{-1}
Root	$K_r^* = 0.0001728$ d^{-1} $K_x = 0.0432$ cm^3 d^{-1}	$K_r^* = 0.001728$ d^{-1} $K_x = 0.432$ cm^3 d^{-1}

† θ_r and θ_s, residual and saturated volumetric water content, respectively; α and n, van Genuchten–Mualem shape parameters; λ, pore connectivity parameter; K_{sat}, saturated hydraulic conductivity.

Table 2). One order of magnitude is indeed a realistic degree of variation for K_{sat} (see, e.g., Javaux and Vanclooster, 2006) and root parameters (Doussan et al., 1998, 2006).

Sensitivity analysis involved comparing the spatial distribution of the sink term, soil water potential, and water content computed for the reference and perturbed parameterizations. This sensitivity analysis was performed for CBCs 1 and 2 (Table 1). We also compared the temporal variations of the collar fluxes, which correspond to the actual transpiration.

Furthermore, an effective one-dimensional sink term was obtained by integrating the local sink terms of the soil voxels located at every depth in the soil profile. One-dimensional variability of the water content and of the velocity field was assessed by computing the CV for each depth. This is of importance for assessing the effect of water extraction on the soil water velocity field and thus on solute transport.

Effect of Soil Type

Soil saturated hydraulic conductivity is not the only soil parameter affecting soil resistance. The complete soil conductivity curve plays a role under unsaturated conditions. To check the effect of soil texture on the water uptake process, we compared the loam soil with two other soils, a clay loam and a clay. Parameters for the clay loam were $\theta_r = 0.095$, $\theta_s = 0.41$, $\alpha = 0.019$ cm^{-1}, $n = 1.31$, and $K_{sat} = 6.24$ cm d^{-1}; and for the clay, $\theta_r = 0.068$, $\theta_s = 0.38$, $\alpha = 0.008$ cm^{-1}, $n = 1.09$, and $K_{sat} = 4.8$ cm d^{-1} (Carsel and Parrish, 1988). For both soils, $m = 1 - 1/n$ and $\lambda = 0.5$. Figure 1 shows the principal hydraulic characteristic functions of these three soils as a function of pF = $\log_{10}(|h|)$, where h is the water potential (cm). The loam had the highest moisture capacity and saturated conductivity, but the steepest decrease with pF. The clay had flatter hydraulic functions and a lower capacity and K_{sat}, whereas the clay loam exhibited intermediate hydraulic properties. Additionally Fig. 1 shows threshold pF values at which the soils had a hydraulic conductivity similar to the root, with root conductivity

TABLE 1. Reference collar boundary conditions (CBCs): geometry, boundary, and initial conditions.

|	CBC 1	CBC 2	CBC 3
Soil			
Geometry	10 by 10 by 40 cm with grid size of 1 by 1 by 1 cm		
Initial conditions	in equilibrium with a 3-m-deep aquifer		
Boundary conditions	no flux at the top, no flux at the bottom		
Root			
Geometry	9488 segments		
Collar boundary condition	constant water potential $h = -1000$ cm	constant potential transpiration $T_{pot} = 0.1563$ cm d^{-1} (water flux at root collar $J_c = 10$ cm^3 d^{-1})	day–night sinusoidal transpiration with maximum $T_{max} = 1.563$ cm d^{-1} and minimum $T_{min} = 0$ cm d^{-1} (max. $J_c = 100$ cm^3 d^{-1})
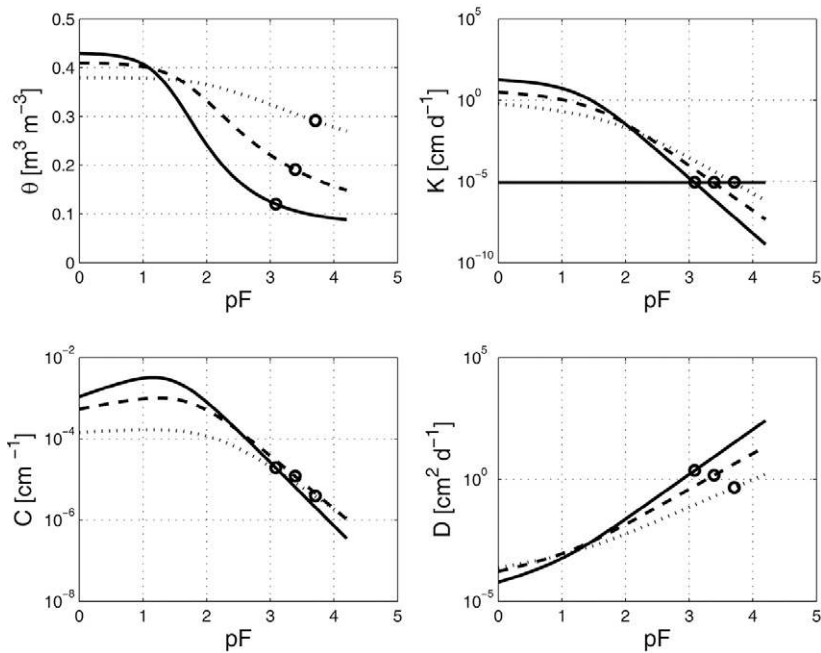
FIG. 1. Water retention (θ), hydraulic conductivity (K), water capacity (C), and water diffusivity (D) for loam (continuous line), clay loam (dashed line), and clay soils (dotted line) as a function of pF = $\log_{10}(|h|)$, where h is the water potential (cm). Root conductivity is given by the gray horizontal line. Open circles characterize the threshold at which the soils and the root have the same hydraulic conductivity.

defined as K_r^* and root radius r = 0.05 cm. Two collar boundary conditions were used for the soil texture sensitivity analysis: CBC 1 and CBC 2 (Table 1).

Effect of the Sinusoidal Day–Night Cycle on Root Water Uptake

A more realistic, sinusoidal day–night scenario was also investigated (CBC 3, Table 1). Maximum transpiration occurred at t = 0.5, 1.5, … d and minimum (zero transpiration) at t = 0, 1, 2, … d. Such a scenario allowed the plant root to experience a large range of collar fluxes and soil water conditions.

Results

Reference Parameterization with Collar Boundary Condition 1

Figure 2 shows typical outputs of R-SWMS after 0.5 d under constant water potential at the root collar (CBC 1). The root structure is shown in the first subplot in white. The second subplot shows that the water potential in the root xylem is mainly controlled by the distance of a root segment from the collar and the number of branches in between. A long root segment without branches and directly connected to the root collar will have a much higher absolute water potential, and thus take up more water, as

long as the conductivity properties are uniform. In the third subplot, the water potential distribution is shown with the water flux streamlines. One may observe that the streamlines are far from horizontal, as usually assumed in two-dimensional root water uptake models. The corresponding water content and three-dimensional sink distributions are given in subplots Fig. 2d and 2e, respectively. The plots show that water is preferably taken up first at lower depths where soil water is still easily available and the gradient between bulk soil and xylem water potentials is still large.

Effect of the Parameterization on the Root Collar Flux

When constant water potential is applied at the root collar (CBC 1), the flow rate at the root collar tends to continuously decrease with time as the soil dries out and the differences between root and soil water potentials diminish. Figure 3 (upper) shows the effect of root and soil hydraulic parameterization on the temporal evolution of the actual flux at the collar, J_c.

Large radial root conductivity dramatically amplifies the initial uptake, whereas a larger xylem conductivity does not exhibit notable differences from the reference parameterization. This illustrates the fact that the principal resistance to water flow is located in the radial root tissues (Steudle and Peterson, 1998). Xylem conductivity is so much larger than radial root conductivity that increasing the former has no effect on water uptake and soil water distribution (see below). When soil hydraulic conductivity is augmented, the temporal course of root collar flux decreases smoothly, probably because of the gradual decrease in the soil hydraulic conductivity with soil drying.
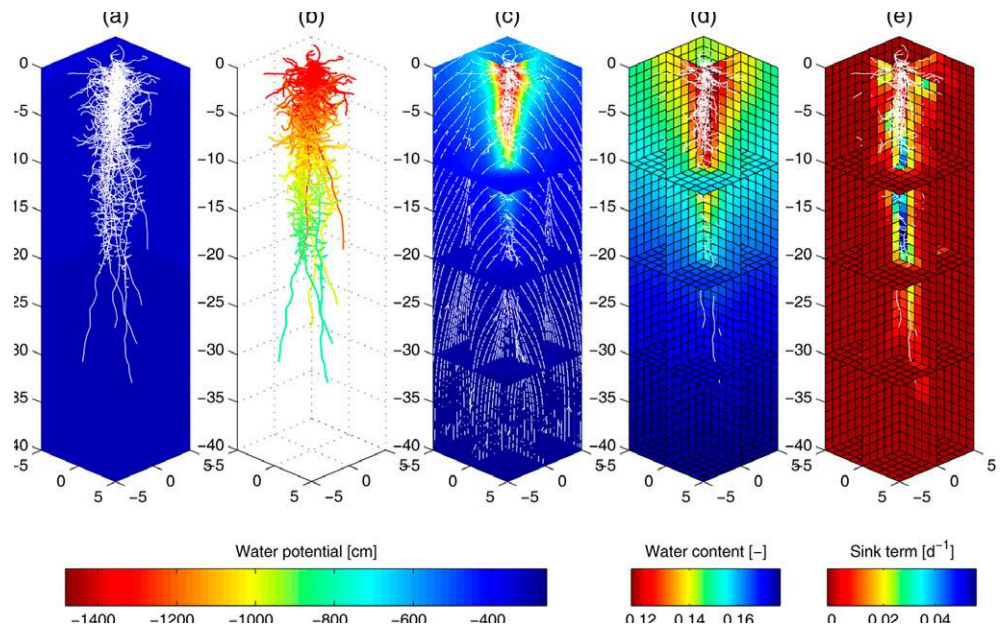

FIG. 2. (a) Root architecture and initial water potential distribution; (b) xylem water potential after 5 d for Collar Boundary Condition 2; (c) soil water potential distribution after 5 d, white arrows show water streamlines; (d) soil water content distribution; and (e) sink term distribution.
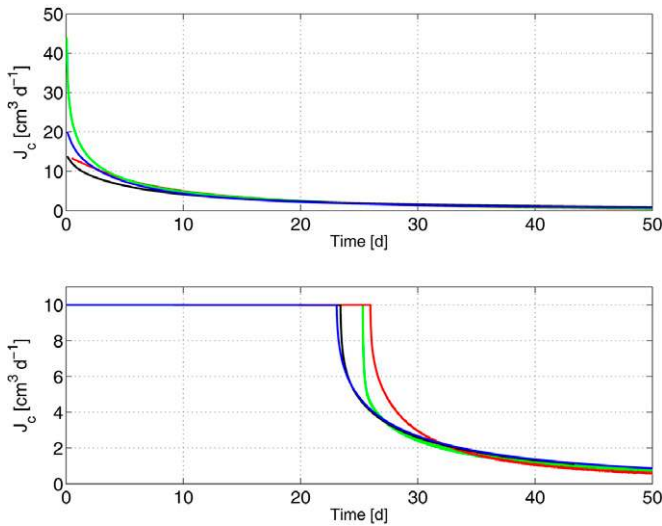
FIG. 3. Time series of the water flow rate at the root collar (J_c) for Collar Boundary Conditions 1 (upper) and 2 (lower). Line colors refer to different root or soil parameterization: reference (black), xylem conductivity multiplied by 10 (blue), radial conductivity multiplied by 10 (green), and soil hydraulic conductivity multiplied by 10 (red).

Figure 3 (lower) corresponds to a constant prescribed water flux at the root collar (CBC 2). Because no water is added to the soil, stress appears after a while when the prescribed flux cannot be fulfilled by the soil, either because of the low hydraulic conductivity or the low capacity of the soil. It is interesting to observe the effect of the hydraulic parameters on the time at which stress appears. Again, no noticeable difference can be observed between the case with larger xylem conductivity and the reference case. On the other hand, stress is delayed for the cases with large soil K_{sat} or

FIG. 4. Cross-sections of the three-dimensional soil water content distribution after 1 d with constant water potential at the root collar h = −1000 cm (Collar Boundary Condition 1, Table 1). Comparison between the reference (extreme right) and 10-fold increase of xylem conductivity (K_x), radial conductance (K_r^*), and saturated soil conductivity (K_s). Root architecture is shown in white.

root K_r^*. The former provides water from other parts of the soil to sustain the water demand around the roots. The latter increases radial flow to the roots, which augments the total amount of water that can extracted by the root before the soil becomes water limiting. When the soil becomes limiting, there is a sudden drop in the collar water flux that cannot be compensated by soil water movement (green line). On the contrary, when K_{sat} is increased, the gradual reduction in soil conductivity creates a smoother decrease of the collar flux (red line); however, this trend depends strongly on the shape of the complete soil hydraulic conductivity curve. This is investigated for the different soils below.

Effect of Parameterization on the Three-Dimensional Distribution of Water Content

Figure 4 shows the soil water distribution after 1 d for CBC 1 (constant water potential at the root collar) together with cases where root radial conductivity K_r^*, xylem axial conductivity K_x, and soil saturated conductivity K_{sat} were multiplied by 10. Basically, almost no differences are observed when the xylem conductivity is increased. In contrast, when radial root conductivity is increased by a factor 10, the water content distribution changes dramatically. This is in line with the observations of water flow at the root collar (see above). A remarkable point is that when the soil conductivity is increased, water uptake is more homogeneously distributed because lateral water fluxes in the soil counteract variability in soil water uptake.

When the same test is performed with flux-type boundary conditions (CBC 2), the parameter perturbations have less impact (Fig. 5). This is because the same amount of water has been extracted for the four cases (due to the same prescribed flux at the collar) and the retention curve is exactly the same in each scenario; however, slight changes in the water distribution can be observed. Again, larger soil conductivity tends to homogenize water distribution while larger xylem conductivity does not have much effect. It is interesting to observe, however, that larger root radial conductivity will decrease the depth but increase the radial distance at which water content distribution is affected: water will be taken up preferentially from the upper layers where less energy is needed to move it to the collar. The resulting water distribution is therefore more circular and almost centered around the root collar.
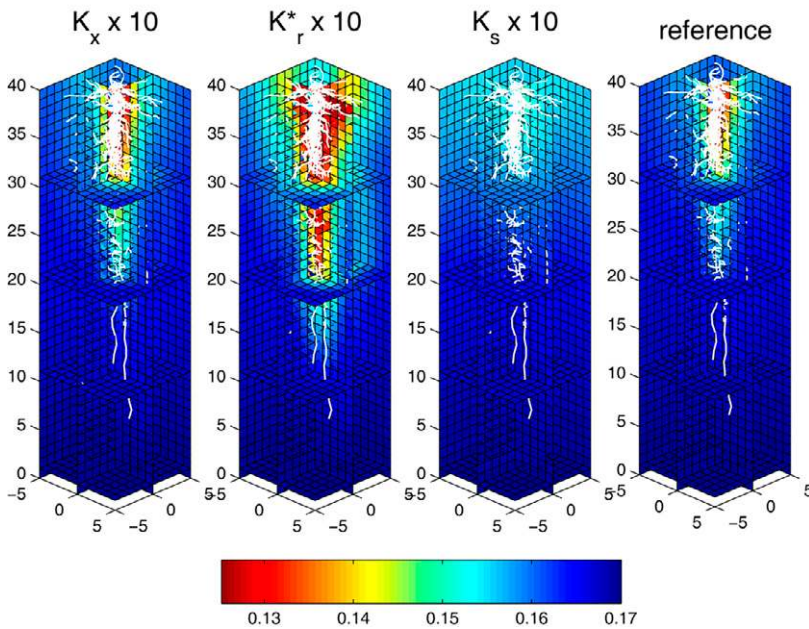
Effect of Parameterization on the Sink-Term Profiles

Figure 6 shows the depth distribution of the root water uptake (similar to a sink-term profile) for CBCs 1 and 2 after 2 d. Except for the high K_{sat} cases (red lines), the sink-term profiles for standard CBCs 1 and 2 already tend to separate from the normalized root length density (RLD) profile. Sink-term and RLD profiles would overlap if the root demand at all depths was instantaneously met by the soil water throughout the profile. This seems not to be the case for the reference, high K_r^*, and high K_x parameterizations, which means that soil resistance already affects the uptake distribution, with soil hydraulic conductivity being lower than root conductivity in the upper soil horizon. The sink-term profile for highly conductive soil
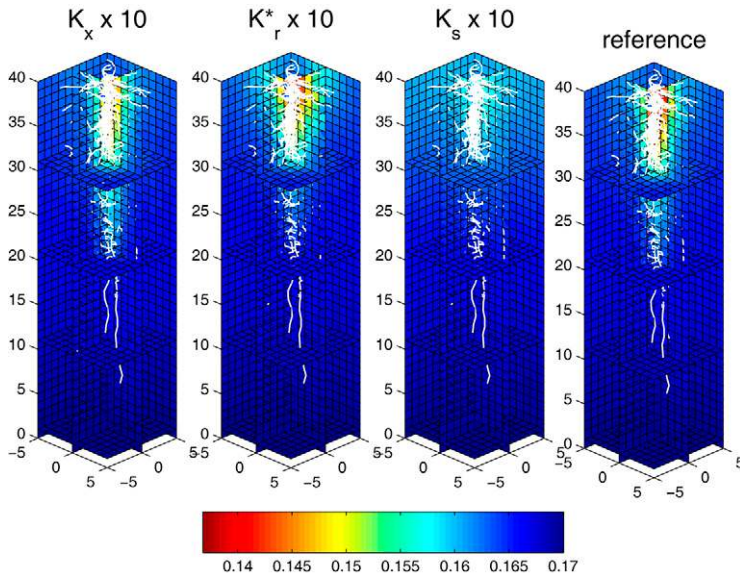
FIG. 5. Cross-sections of the three-dimensional soil water content distribution after 7 d with constant water flux at the root collar $J_c = -10$ cm³ d⁻¹ (Collar Boundary Condition 2, Table 1). Comparison between the reference (extreme right) and 10-fold increase of xylem conductivity(K_x), radial conductance (K_r^*), and saturated soil conductivity (K_s). Root architecture is shown in white.
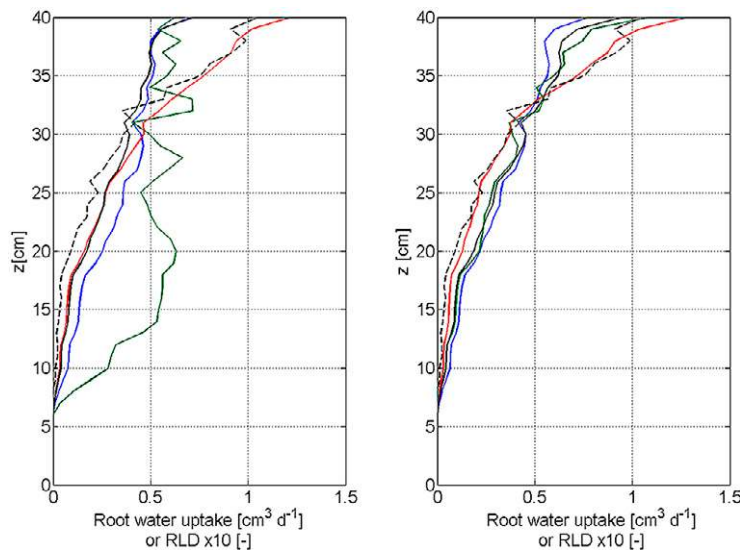

FIG. 6. Sink-term profile for Collar Boundary Condition 1 (left) and 2 (right). Line colors refer to different root or soil parameterization: reference (black), xylem conductivity multiplied by 10 (blue), radial conductivity multiplied by 10 (green), and soil hydraulic conductivity multiplied by 10 (red). For clarity, the dashed line represents the normalized root length density (RLD) profile multiplied by 10.

is stabilized because water from wetter parts of the soil continuously compensate for soil water extraction from the top layer (red lines).

Because more water is extracted when xylem resistance is lowered for CBC 1, the water has to be taken up from deeper layers, which renders the sink-term profile more uniform with depth and different from the RLD profile (blue line, left subplot). The same behavior, but to an even larger extent, is observed when the radial conductance is augmented (green line, left subplot).

On the other hand, for CBC 2, augmenting the radial and xylem conductivities does not dramatically affect the sink-term profile. For low flow at the root collar (far away from stress conditions), it appears that the soil governs the depth distribution of root water uptake, which is slightly different than the RLD profile.

Effect of Parameterization on the Vertical Distribution of Water Content and Flow Velocity Field

Despite important differences between sink-term profiles for CBCs 1 and 2 with different parameterizations (Fig. 6), the corresponding one-dimensional water content profiles almost overlap, except for the high K_r^* case (Fig. 7, top). The water content distributions are smoothed out relative to the sink-term profiles due to vertical and horizontal redistribution between voxels, as shown by the averaged horizontal and vertical components of the velocity profiles (Fig. 7, middle and bottom). Redistribution is particularly visible when K_{sat} is increased (red lines). In such a case, water from other soil layers compensates, as illustrated by the large vertical velocity component (Fig. 7, bottom). This type of redistribution may bring into question the usual assumption that changes in water content profiles correspond to the sink-term profile and that the flow streamlines are principally horizontal.

Figure 8 shows the CVs of the water content and of the vertical and horizontal components of the velocity field throughout the soil profile. These factors characterize the degree of water distribution heterogeneity induced by root water uptake. This information is crucial for solute transport prediction at the plant scale, as it will affect the dispersivity length. In general, Fig. 8 shows that parameterization has a nonnegligible impact on water content and flux distribution. This information is similar to that typically obtained with geophysical tomography and could help interpret experimental measurements of uptake processes.

Although CBC 2 generates for each parameterization the same amount of extracted water for the first 7 d, the parameterization affects water variability. This contrasts with the previous observation that the different parameterizations produce similar sink terms (Fig. 6b). The high K_{sat} cases (red dashed lines in Fig. 8) generate low variability in water content because soil water fluxes compensate for local root water.

The results suggest that three-dimensional water content maps combined with plant transpiration monitoring could give valuable information on root–soil interactions and the relative importance of the different resistances along the water flow pathway. Thus, novel geophysical applications like nuclear magnetic resonance (Pohlmeier et al., 2007, 2008) or small-scale electrical resistivity tomography that allow monitoring three-dimensional moisture variability could be combined with detailed three-dimensional models to characterize water uptake processes and plant parameters.

Effect of Soil Type

The root collar fluxes under CBCs 1 and 2 for the three soil types described in Fig. 1 are shown in Fig. 9. For CBC 2, we observe that stress appeared first for loam, then for clay, and eventually for the clay loam soil. For CBC 1, the clay loam generated
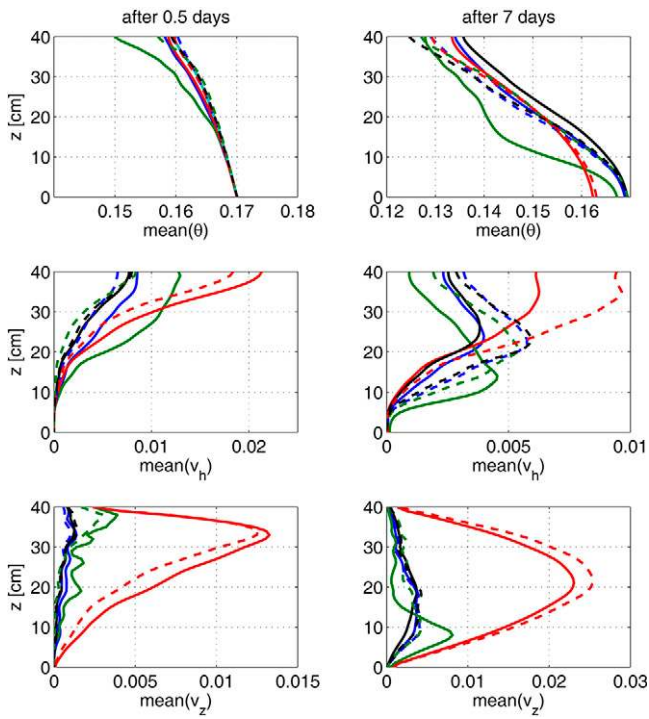
FIG. 7. Averaged water content (θ) profile, averaged horizontal component of the velocity field (v_h) profile, and averaged vertical component of the velocity field (v_z) profile after 0.5 and 7 d for Collar Boundary Conditions 1 (continuous lines) and 2 (dashed lines). Line colors refer to different root or soil parameterization: reference (black), xylem conductivity multiplied by 10 (blue), radial conductivity multiplied by 10 (green), and soil hydraulic conductivity multiplied by 10 (red).
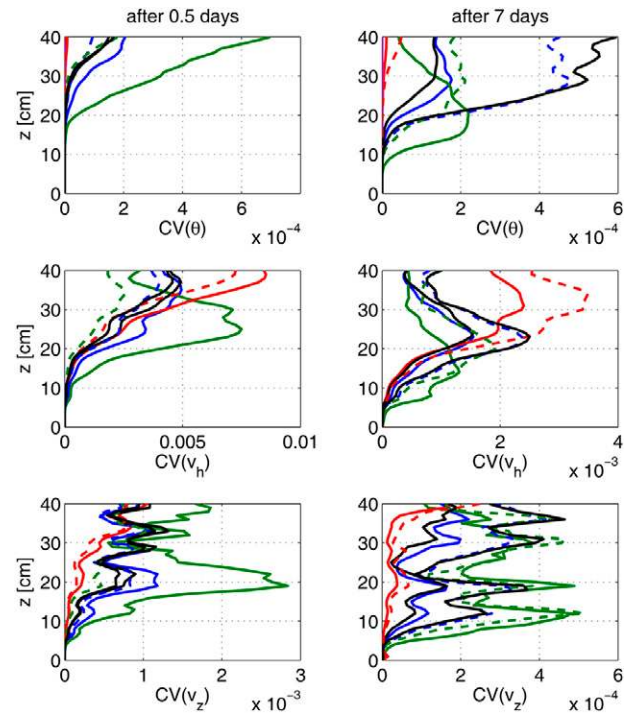

FIG. 8. Water content variability profile [CV(θ)] and coefficients of variability of the horizontal component of the velocity field profile [CV(v_z)] and the horizontal component of the velocity field profile [CV(v_h)] after 0.5 and 7 d for Collar Boundary Conditions 1 (continuous lines) and 2 (dashed lines). Line colors refer to different root or soil parameterization: reference (black), xylem conductivity multiplied by 10 (blue), radial conductivity multiplied by 10 (green), and soil hydraulic conductivity multiplied by 10 (red).
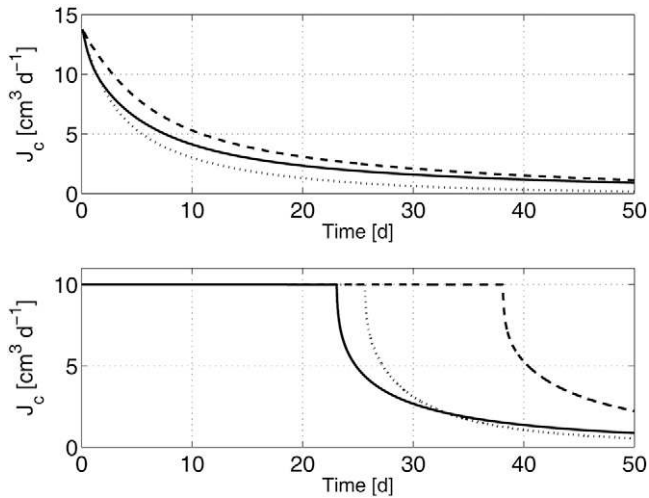

FIG. 9. Time series of the water flux at the root collar (J_c) for Collar Boundary Conditions 1 (upper) and 2 (lower). Continuous lines refer to loam, dashed lines to clay loam, and dotted lines to clay soils.
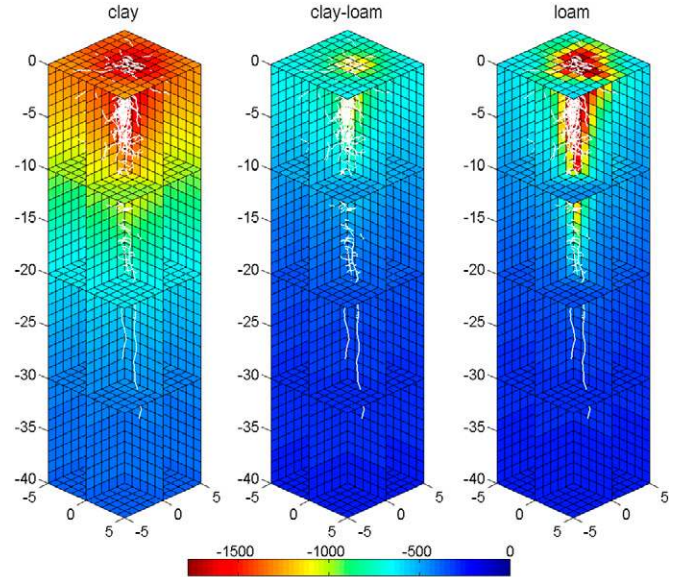

FIG. 10. Cross-sections of the three-dimensional water potential distribution after 7 d with constant water flux at the root collar (Collar Boundary Condition 1, Table 1) for the three soil types. Root architecture is shown in white.

the largest water extraction. This illustrates that K_{sat} alone cannot be used to predict a priori the soil behavior when plants are present. The shape of the conductivity and retention is also of interest. Figure 10 shows the water potential distribution after 7 d under a constant-flux CBC. While the water potential distributions for the clay and clay loam soils were rather homogeneous in the horizontal direction, the loam had a heterogeneous, three-

dimensional distribution, with very dry soil surrounding the main root axes and wetter soil away from the roots. The steeper slope of the loam hydraulic properties generated a larger conductivity drop, which produced early stress. This is confirmed in Fig. 11,
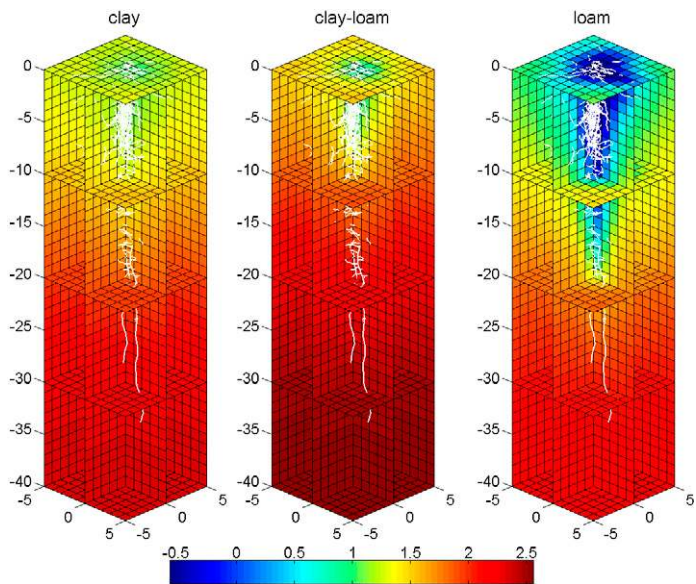
FIG. 11. Cross-sections of the three-dimensional distribution of the ratio between soil and root conductivity ($\log_{10}[K(h)/K_r]$) after 7 d with constant water flux at the root collar (Collar Boundary Condition 2, Table 1) for the three soil types. Root architecture is shown in white.

FIG. 12. Profile of the sink term for the standard Collar Boundary Condition 3.

where the distribution of the soil and root conductivity ratio is shown (logarithmic scale) after 7 d for CBC 2, which is much before the onset of substantial stress (h at the root collar equals $h_{\lim}$). Values below zero indicate that the soil is less conductive than the radial root pathway. While the voxels around the roots were already limiting plant uptake at the upper depth for the loam soil, the clay and clay loam soils were still nonlimiting at all depths.

The fact that stress was generated earlier for clay than for clay loam is due to the fact that clay has a much lower capacity, defined here as the water available for plant uptake between $h = 0$ and $h = h_{\lim}$. Therefore, after 7 d, the soil was already very dry (Fig. 10). Yet, in contrast to the loamy soil, the water potential distribution in the clay was quite uniform in the horizontal direction due to the fact that the hydraulic conductivity under low potential was higher than for the loam soil (see Fig. 1). Figure 11 clearly shows that after 7 d the soil conductivity around root segments was much higher for the clay than for the loam.

The clay loam soil appears to have the best hydraulic properties to sustain the evaporative demand, whatever the CBC (Fig. 10). Its high capacity combined with its relatively high hydraulic conductivity across a wide range of pF values allowed the clay loam to support the evaporative demand for 15 d more than the loam (Fig. 9). This outcome was not apparent beforehand from the soil and root properties alone because the clay loam hydraulic properties appeared to be intermediate between clay and sand (Fig. 1). The result points out the usefulness of three-dimensional models like R-SWMS for investigating root water uptake and various assumptions made by simplified one-dimensional models.

Day–Night Scenario

Figure 12 shows the sink-term profiles for different times under day–night cycles (CBC 3) with the reference parameterization for loam (Tab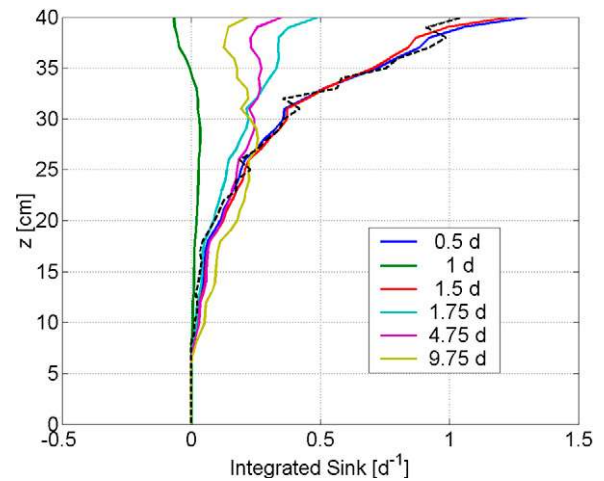le 2). Maximum transpiration occurred at $t =$ 0.5, 1.5, … d and minimum (zero transpiration) at $t = 0, 1, 2,$ … d. The figure shows that sink-term profiles corresponding to maximum transpiration overlap the RLD profile at the beginning of the experiment but that after 9.75 d, plants extracted water from lower depths. During the night (zero transpiration), a "negative" sink term was observed for upper depths, while lower depths remained positive. This is consistent with the concept of "hydraulic lift" (Dawson, 1993), which has been observed in experiments under dry climates. At night, the water potential gradient may be reversed in the upper soil (absolute water potential lower in the soil than in the plant), which produces water release from the root to the soil. Hydraulic lift is possibly a mechanism by which a plant can bring water to the upper soil layers during the night and then use that water to help satisfy transpiration demand the following day. Certain plants may have mechanisms for decreasing radial conductivity and preventing such water releases (Vandeleur et al., 2005).

Effective Sink Term as a Function of Bulk Water Potential and Averaged Water Content

To assess the effect of the soil on root water uptake, a dimensionless sink term may be used that is a function of the soil water potential. The effects of the soil and the roots are usually considered to be independent and the sink term is written as (e.g., Feddes and Raats, 2004)

$$S(z,t) = \alpha_1(h,\theta,z)\,g(z)\,T_{\text{pot}}(t) \qquad [4]$$

where T_{pot} is the potential transpiration or the maximum non-stressed water extraction rate [L T^{-1}], $g(z)$ is the normalized root distribution function [L^{-1}], and α_1 is a function that characterizes the effect of the soil (stress function).

To generate a comparable function, we used the day–night CBC 3 with a high transpiration amplitude that generated a wide range of J_c values (Table 2). The simulated high evaporative demand could not be met and water stress was rapidly induced, decreasing the actual flux at the root collar during the third day (Fig. 13).

As shown in Fig. 14, we estimated for each depth the averaged bulk water potential or water content and plotted them vs. both the normalized sink term [$S^*(z,t) = S(z,t)/T_{\text{pot}}$] and
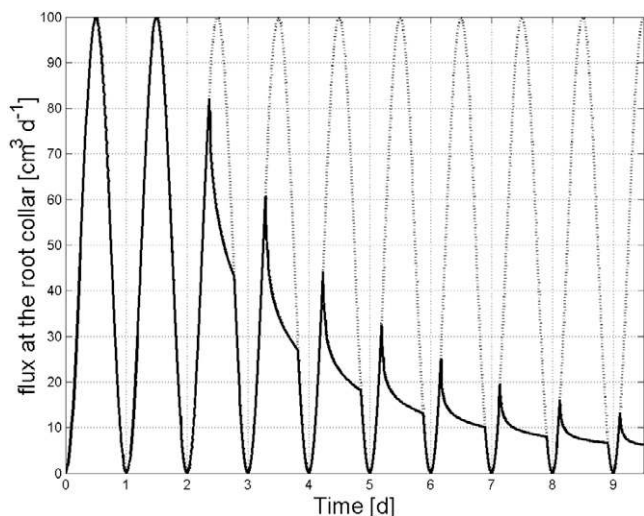
FIG. 13. Prescribed (dashed line) and actual (continuous line) flux at the root collar under Collar Boundary Condition 3 with 10 times larger maximum transpiration.

the normalized sink term divided by the root surface density [$S^*(z,t)/g(z,t)$]. Each open circle in the plots represents a pair (S^*,θ) or (S^*,h) at a given time. The plots do not resemble monotonic functions traditionally used for α_1, such as the Feddes et al. (1977) model that has a plateau with maximum uptake between two reduction points. This is quite surprising given the large number of studies devoted to characterizing one-dimensional relationships between sink and soil water status. Here it is observed that the soil plays a big role even at low absolute water potential, while usually it is assumed that the soil is important only beyond a certain water potential. On the other hand, sink variability is higher for water potential values close to zero, where root is limiting and where water uptake is more related to depth and soil water potential. For a given value of (averaged) h or θ, there are plenty of possible sinks depending on the root boundary condition and soil status. This indicates that simple Feddes-like reduction functions, which are not based on biophysical processes, may not be generally applicable across climates and soil types.

Conclusions

In this study, we have shown with simple scenarios the important complexity of the root water uptake process when modeled in three dimensions based on the water potential gradient between soil and roots. The relative radial root conductivity and the distribution of soil hydraulic conductivity, which depends on water content and the soil moisture capacity, were shown to control the plant water extraction distribution.

Highly conductive soils promote water uptake but at the same time decrease variability in soil water content. Variability arising from root uptake is reduced by large lateral and vertical soil water fluxes. The uptake profile produced by these conditions matches the root density profile as long as sufficient water remains in the soil. Large root radial conductance increases the amount of water extracted by the root under given collar conditions. Under these conditions, however, the water extraction will not follow to the root distribution. As long as the xylem conductivity is everywhere high enough to conduct all the extracted water, soil water

extraction patterns are relatively insensitive to further increases in xylem conductivity.

It was also shown that the slope of the retention and conductivity curves between saturation and the limiting water potential is crucial for predicting root water uptake. A soil with high K_{sat} and large capacity can quickly become limiting for root water uptake if its hydraulic conductivity curve is steep. In contrast, a soil with lower capacity and smaller K_{sat} but with a relatively flat conductivity curve can support a given evaporative demand much longer before reaching stress conditions. No simple rules about optimal soils for root water uptake, however, can be deducted a priori from the soil hydraulic properties because it depends on the evaporative demand and on the three-dimensional distribution of the root/soil conductivity ratio and on the soil moisture capacity. This issue is currently being investigated further.

It was also shown that similar sink-term profiles could result in very different water content and flux distributions at the plant scale due to the relative magnitudes of soil and root hydraulic properties. The complexity of the variability means that three-dimensional models such as R-SWMS are key tools for improving the understanding of water variability and solute transport at the plant scale. At larger scales, however, other factors like row position (Hupet and Vanclooster, 2005) or heterogeneity of plant species (Nordbotten et al., 2006) may be crucial for the spatial variability of water.

Interactions of soil and root hydraulic properties lead to very complex $S(h)$ or $S(\theta)$ relationships, very different from the simple Feddes-like stress functions usually found in the literature. It appears that simple one-dimensional sink terms have a limited biophysical basis, making it difficult if not impossible to extrapolate such traditional reduction functions to other climatic conditions and soil types. It is possible that traditional one-dimensional sink terms could be related to the outer envelope
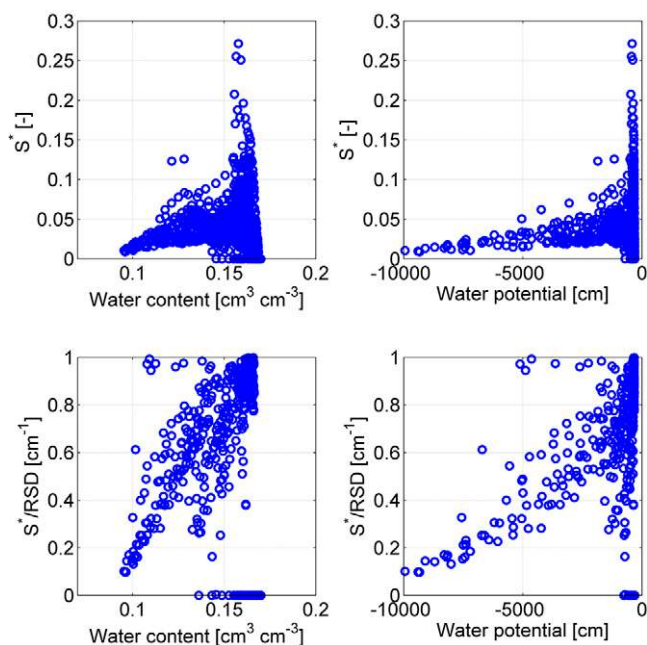

FIG. 14. Normalized sink term (S^*) vs. averaged water content (upper left) and averaged bulk water potential (upper right), and S^* divided by the root surface density (RSD) vs. averaged water content (lower left) and averaged bulk water potential (lower right).

of the true $S^*(h)$ or $S^*(\theta)$ relationships, something that could be investigated in the future with R-SWMS.

It is worth noting that numerous assumptions were made in this study. The effects of the root property distribution, root growth, and soil heterogeneity were neglected. We assumed that the water was taken up passively by the plant and that the soil and root properties were constant. The averaging procedure of the subscale water potential distribution around roots in R-SWMS can also be improved (Schröder et al., 2008).

Finally, developing such a detailed model does not make sense if no comparison with experiments is possible. Emerging imaging techniques, such as nuclear magnetic resonance, should make that comparison possible (Pohlmeier et al., 2008). The next step is to investigate the potential of these new imaging methods to improve the parameterization of such detailed three-dimensional models.

References

Bruckler, L., F. Lafolie, C. Doussan, and F. Bussieres. 2004. Modeling soil–root water transport with non-uniform water supply and heterogeneous root distribution. Plant Soil 260:205–224.

Carsel, R.F., and R.S. Parrish. 1988. Developing joint probability distributions of soil water retention characteristics. Water Resour. Res. 24:755–769.

Clausnitzer, V., and J.W. Hopmans. 1994. Simultaneous modeling of transient 3-dimensional root-growth and soil-water flow. Plant Soil 164:299–314.

Cowan, I.R. 1965. Transport of water in the soil–plant–atmosphere system. J. Appl. Ecol. 2:221–239.

Dawson, T. 1993. Hydraulic lift and water-use by plants: Implications for water balance, performance and plant–plant interactions. Oecologia 94:565–574.

de Dorlodot, S., B. Forster, L. Page, A. Price, R. Tuberosa, and X. Draye. 2007. Root system architecture: Opportunities and constraints for genetic improvement of crops. Trends Plant Sci. 12:474–481.

de Jong van Lier, Q., K. Metselaar, and J.-C. van Dam. 2006. Root water extraction and limiting soil hydraulic conditions estimated by numerical simulation. Vadose Zone J. 5:1264–1277.

Doussan, C., L. Pages, and G. Vercambre. 1998. Modelling of the hydraulic architecture of root systems: An integrated approach to water absorption—Model description. Ann. Bot. 81:213–223.

Doussan, C., A. Pierret, E. Garrigues, and L. Pages. 2006. Water uptake by plant roots: II. Modelling of water transfer in the soil root-system with explicit account of flow within the root system: Comparison with experiments. Plant Soil 183:99–117.

Feddes, R.A., and P.A.C. Raats. 2004. Parameterizing the soil–water–plant root system. p. 95–141. In R.A. Feddes et al. (ed.) Unsaturated-zone modeling: Progress, challenges, applications. UR Frontis Ser. 6. Kluwer Acad. Press, Wageningen, The Netherlands.

Feddes, R.A., H. Zaradny, and P. Kowalik. 1977. Simulation of evapotranspiration with different root water-uptake functions. Trans. Am. Geophys. Union 58:900.

Fitter, A.H. 1987. An architectural approach to the comparative ecology of plant-root systems. New Phytol. 106:61–77.

Gardner, W.R. 1960. Dynamic aspects of water availability to plants. Soil Sci. 89:63–73.

Garrigues, E., C. Doussan, and A. Pierret. 2006. Water uptake by plant roots: I. Formation and propagation of a water extraction front in mature root systems as evidenced by 2D light transmission imaging. Plant Soil 283:83–98.

Green, S., M. Kirkham, and B. Clothier. 2006. Root uptake and transpiration: From measurements and models to sustainable irrigation. Agric. Water Manage. 86:165–176.

Hupet, F, and M. Vanclooster. 2005. Micro-variability of hydrological processes at the maize row scale: Implications for soil water content measurements and evapotranspiration estimates. J. Hydrol. 303:247–270.

Javaux, M., and M. Vanclooster. 2006. Scale-dependency of the hydraulic properties of a variably saturated heterogeneous sandy subsoil. J. Hydrol. 327:376–388.

Lynch, J. 1995. Root architecture and plant productivity. Plant Physiol. 109:7–13.

Nordbotten, J.M., I. Rodriguez-Iturbe, and M.A. Celia. 2006. Non-uniqueness of evapotranspiration due to spatial heterogeneity of plant species. Proc. R. Soc. A 462:2359–2371.

Pierret, A., C. Doussan, Y. Capowiez, F. Bastardie, and L. Pages. 2007. Root functional architecture: A framework for modeling the interplay between roots and soil. Vadose Zone J. 6:269–281.

Pohlmeier, A., A. Oros-Peusquens, M. Javaux, M. I. Menzel, J. Vanderborght, J. Kaffanke, S. Romanzetti, J. Lindenmair, H. Vereecken, and N.J. Shah. 2008. Changes in soil water content resulting from *Ricinus* root uptake monitored by magnetic resonance imaging. Vadose Zone J. 7:1010–1017 (this issue).

Pohlmeier, A., A.M. Oros-Peusquens, M. Javaux, M.I. Menzel, H. Vereecken, and N.J. Shah. 2007. Investigation of water content and dynamics of a *Ricinus* root system in unsaturated sand by means of SPRITE and CISS: Correlation of root architecture and water content change. Magn. Reson. Imaging 25:579–580.

Schröder, T., M. Javaux, J. Vanderborght, B. Koerfgen, and H. Vereecken. 2008. Effect of local soil hydraulic conductivity drop on using a three-dimensional root water uptake model. Vadose Zone J. 7:1089–1098 (this issue).

Simunek, J., K. Huang, and M.Th. van Genuchten. 1995. The SWMS_3D code for simulating water flow and solute transport in three-dimensional variably-saturated media. Version 1.0. Res. Rep. 139. U.S. Salinity Lab., Riverside, CA.

Somma, F., J.W. Hopmans, and V. Clausnitzer. 1998. Transient three-dimensional modeling of soil water and solute transport with simultaneous root growth, root water and nutrient uptake. Plant Soil 202:281–293.

Steudle, E., and C.A. Peterson. 1998. How does water get through roots? J. Exp. Bot. 49:775–788.

Vandeleur, R., C. Niemietz, J. Tilbrook, and S.D. Tyerman. 2005. Roles of aquaporins in root responses to irrigation. Plant Soil 274:141–161.

Vrugt, J.A., M.T. van Wijk, J.W. Hopmans, and J. Šimunek. 2001. One-, two-, and three-dimensional root water uptake functions for transient modeling. Water Resour. Res. 37:2457–2470.